

Communication

# Synthesis, Structural, and Magnetic Characterization of a Mixed 3d/4f 12-Metallacrown-4 Family of Complexes

Angeliki A. Athanasopoulou <sup>1,2</sup>, Luca M. Carrella <sup>1</sup> and Eva Rentschler <sup>1,\*</sup>

<sup>1</sup> Institute of Inorganic and Analytical Chemistry, Johannes Gutenberg University Mainz, Duesbergweg 10-14, D-55128 Mainz, Germany; aathanas@uni-mainz.de (A.A.A.); carrella@uni-mainz.de (L.M.C.)

<sup>2</sup> Graduate School Materials Science in Mainz, Staudinger Weg 9, D-55128 Mainz, Germany

\* Correspondence: rentschler@uni-mainz.de; Tel.: +49-613-1392-5491

Received: 21 June 2018; Accepted: 5 July 2018; Published: 7 July 2018



**Abstract:** A new family of complexes (<sup>t</sup>Bu<sub>4</sub>N){[Ln<sup>III</sup>(O<sub>2</sub>CBu<sup>t</sup>)<sub>4</sub>][12-MC-Mn(III)N(shi)-4]}·5CH<sub>2</sub>Cl<sub>2</sub> (Ln = Gd (**1**) and Tb (**2**)), (<sup>t</sup>Bu<sub>4</sub>N)<sub>2</sub>{[Y<sup>III</sup>(O<sub>2</sub>CBu<sup>t</sup>)<sub>4</sub>][12-MC-Mn(III)N(shi)-4]}(ClO<sub>4</sub>) (**3**); where shiH<sub>3</sub> = salicylhydroxamic acid; Bu<sup>t</sup>CO<sub>2</sub><sup>−</sup> = pivalate ions; <sup>t</sup>Bu<sub>4</sub>N = tetrabutylammonium and ClO<sub>4</sub><sup>−</sup> = perchlorate ions, has been isolated. The reaction of salicylhydroxamic acid with Mn(O<sub>2</sub>CBu<sup>t</sup>)<sub>2</sub>·2H<sub>2</sub>O, Ln(NO<sub>3</sub>)<sub>3</sub>·xH<sub>2</sub>O, <sup>t</sup>Bu<sub>4</sub>NClO<sub>4</sub> in the presence of morpholine (C<sub>4</sub>H<sub>9</sub>NO) led to the isolation of compounds **1–3**. The complexes belong to the 12-MC-4 family of Metallacrowns (MCs) possessing a central {Mn<sub>4</sub><sup>III</sup>Ln<sup>III</sup>(μ-NO)<sub>4</sub>}<sup>11+</sup> core with the four Mn<sup>III</sup> atoms occupying the periphery positions, while the formed [Mn–N–O] repeating unit, assists in the accommodation of the Ln<sup>III</sup> atom in the center of the ring. Peripheral ligation is provided by four η<sup>1</sup>:η<sup>1</sup>:μ pivalate ions. Direct current magnetic susceptibility (dc) measurements revealed the presence of predominant antiferromagnetic exchange interactions within the metal centers. A 1-*J* fitting model was used in order to quantify the Mn<sup>III</sup>–Mn<sup>III</sup> interactions and fitting of the data, for the diamagnetic Y<sup>III</sup> analogue, gave *J* = −3.74 cm<sup>−1</sup> and *g*<sub>Mn(III)</sub> = 2.07. Fitting of the {Mn<sub>4</sub>Gd} compound using a 2-*J* model, counting additionally for the Mn<sup>III</sup>–Gd<sup>III</sup> interactions, revealed values of *J*<sub>1</sub> = −3.52 cm<sup>−1</sup>, *J*<sub>2</sub> = −0.45 cm<sup>−1</sup>, and *g*<sub>Mn(III)</sub> = 1.99.

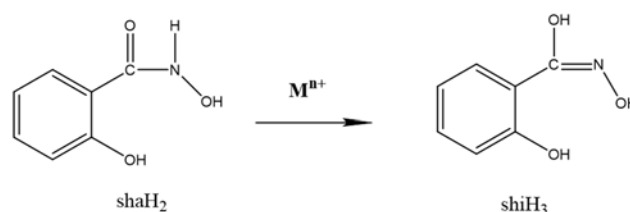
**Keywords:** metallacrowns; single-molecule magnets (SMMs); heterometallic complexes; inorganic synthesis; coordination chemistry

## 1. Introduction

Heterometallic 3d/4f complexes continue to attract the interest of the scientific community as they have been proven to be good candidates for possible applications in various fields such as optics [1,2], catalysis [3], and molecular magnetism [4]. In the field of molecular magnetism, the use of paramagnetic 3d metal ions in combination with highly anisotropic lanthanides such as Dy<sup>III</sup> or Tb<sup>III</sup> with large and unquenched orbital angular momenta [5] can lead to single-molecule magnetism (SMM) behavior with large anisotropy barriers (or energy barriers) for the magnetization reversal. In a common understanding, an SMM is able to retain its magnetization only as long as it is kept below a characteristic blocking temperature, *T*<sub>B</sub>, in the absence of an applied magnetic field [6]. The magnitude of the energy barrier to spin reversal (*U*<sub>eff</sub>) in 3d SMMs is equal to *S*<sup>2</sup> |*D*| for integer and (*S*<sup>2</sup> − 1/4) |*D*| for half-integer spin systems, where *D* is the zero-field splitting parameter. Thus, the total spin of the molecule, *S*, and the Ising-type magnetic anisotropy, are the two factors that block the magnetization reversal. In transition metal complexes, the ground state bistability arises from the total spin *S* with the ensuing [2*S* + 1] *m*<sub>s</sub> microstates, while in lanthanides, the spin-orbit-coupled ground

term  $2S+1L_J$  splits into  $[2J + 1] m_J$  microstates that are responsible for the magnetic bistability of those complexes [5]. Experimentally, we can detect the slow magnetic relaxation of SMMs by performing alternating-current (ac) susceptibility measurements and, most importantly, by the observation of hysteresis loops, which is the ultimate diagnostic property of bulk classical magnets [7]. Recently, quantum tunneling of magnetization (QTM) [8,9] and quantum interference promote the discussion of SMMs as being ideal candidates for even more advanced applications such as spintronics and quantum computing [9–11].

Metallacrowns (MCs) is a class of compounds that since their discovery has attracted the immense attention of the scientific community [12–14]. Most of these complexes have repeatedly demonstrated their ability to encapsulate a central metal ion in their MC cavity, similar to crown ethers, and till now a wide range of MC sizes has been reported [15]. The first example of a 12-MC-4 was reported in 1989 by Pecoraro and Lah, and it was a  $Mn(OAc)_2[12-MC_{Mn^{III}(N)shi}-4]$  complex where  $OAc^-$  is acetate ions and  $shi^{3-}$  is salicylhydroximate ions [13]. Pecoraro and coworkers have exceedingly demonstrated that salicylhydroxamic acid ( $shaH_2$ , Scheme 1) can possibly be subjected to a metal-assisted 2-amide-iminol tautomerism, which leads to salicylhydroxime ( $shiH_3$ , Scheme 1); the latter being an excellent chelating-bridging ligand which has also been shown to possess the appropriate geometry to afford the 12-MC-4 motif [1,15]. The formed repeating unit of  $[Mn^{III}-N-O]$ , along with the triply deprotonated salicylhydroximate, the central  $Mn^{II}$  ion and the two acetate bridges were responsible for the aforementioned configuration. Usually, in the central MC cavity sits a transition metal ion, even though there are also reports where alkali and alkaline earth metals occupy the cavity [15,16]. Lately, the focus has been turned into the incorporation of lanthanide ions in the center, since these compounds have been proposed as excellent candidates for molecular recognition [17,18], molecular magnetism [19] and luminescent [1,19–22] technologies.



**Scheme 1.** Illustrative representation and abbreviation of organic molecules discussed in the text.

Although there have been numerous 12-MC-4 complexes reported to date, only a few comprise the  $3d/4f$  motif with salicylhydroxamic acid ( $shiH_3$ ) [23–25]. If we further restrict the above requirements, by exclusively using  $Mn^{III}$  as the periphery ring metal ion, only a very few papers have been published featuring the above qualifications. Pecoraro and Zaleski reported a complex with the general formula being  $Ln^{III}M^I(OAc)_4[12-MC_{Mn^{III}(N)shi}-4](H_2O)_4 \cdot 6DMF$  where  $M^I = Na^I$  and  $K^I$ , and  $Ln =$  various lanthanides [26–28]. This family of compounds has been extensively structurally studied but the authors did focus their investigations mainly towards the effect that the  $Na^I$  or  $K^I$  ions had on magnetic measurements and not on the pure  $\{Mn_4^{III}Ln^{III}(\mu-NO)_4\}^{11+}$  magnetic core, without emphasizing on the evaluation of exchange interactions by fitting of the data. Our group has a great interest in the synthesis and magnetic characterization of MCs and so far has dealt with the isolation of homometallic and heterometallic ones based on transition metal ions [29–32]. Herein, we report the synthesis, crystal structures and magnetic studies of a rare family of isostructural  $(^tBu_4N)\{[Ln^{III}(O_2CBu^t)_4][12-MC_{Mn^{III}(N)shi}-4]\} \cdot 5CH_2Cl_2$  ( $Ln = Gd$  (1) and  $Tb$  (2)) and a  $(^tBu_4N)_2\{[Y^{III}(O_2CBu^t)_4][12-MC_{Mn^{III}(N)shi}-4]\} \cdot (ClO_4)$  (3) compound. This is an unprecedented example of  $Ln(III)[12-MC_{Mn^{III}(N)shi}-4]$  without the presence of any alkali or alkaline earth metals.

## 2. Results and Discussion

### 2.1. Crystal Structures of Compounds 1–3

The general reaction of  $\text{Mn}(\text{O}_2\text{CBu}^t)_2 \cdot 2\text{H}_2\text{O}$ ,  $\text{M}(\text{NO}_3)_3 \cdot x\text{H}_2\text{O}$  ( $\text{M} = \text{Gd}^{\text{III}}$ ,  $\text{Tb}^{\text{III}}$ ,  $\text{Y}^{\text{III}}$ ),  $\text{shaH}_2$ ,  ${}^t\text{Bu}_4\text{NClO}_4$  and morpholine, in a 4:1:4:1:4 molar ratio, in  $\text{CH}_2\text{Cl}_2$  gave dark brown solutions which were layered with hexanes to give dark brown crystals of  $({}^t\text{Bu}_4\text{N})\{[\text{Ln}^{\text{III}}(\text{O}_2\text{CBu}^t)_4][12\text{-MC-}_{\text{Mn}(\text{III})\text{N}(\text{shi})^{-4}}]\} \cdot 5\text{CH}_2\text{Cl}_2$  (or  $({}^t\text{Bu}_4\text{N})[\text{Mn}^{\text{III}}_4\text{Ln}^{\text{III}}(\text{O}_2\text{CBu}^t)_4(\text{shi})_4] \cdot 5\text{CH}_2\text{Cl}_2$ ) for **1** and **2** and  $({}^t\text{Bu}_4\text{N})_2\{[\text{Y}^{\text{III}}(\text{O}_2\text{CBu}^t)_4][12\text{-MC-}_{\text{Mn}(\text{III})\text{N}(\text{shi})^{-4}}]\} \cdot (\text{ClO}_4) \cdot ({}^t\text{Bu}_4\text{N})_2[\text{Mn}^{\text{III}}_4\text{Ln}^{\text{III}}(\text{O}_2\text{CBu}^t)_4(\text{shi})_4] \cdot (\text{ClO}_4)$  for **3** in high yields (>59%). The chemical and structural identities of the compounds were confirmed by single-crystal X-ray crystallography, elemental analyses (C, H, N) and IR spectral data (Supplementary Materials).

Single-crystal diffraction studies revealed that compounds **1** and **2** are isostructural and crystallize in the  $P4/n$  tetragonal space group, while complex **3** crystallizes in the  $P4cc$  tetragonal space group (Table S1). Although complex **3** is not isostructural with complexes **1** and **2**, still it does possess the same core with them and thus, only complex **2** will be thoroughly described for simplicity reasons. The structure of **2** consists of a  $[\text{Tb}^{\text{III}}(\text{O}_2\text{CBu}^t)_4][12\text{-MC-}_{\text{Mn}(\text{III})\text{N}(\text{shi})^{-4}}]^-$  anion (Figure 1), one  ${}^t\text{Bu}_4\text{N}^+$  cation and, five non-coordinated  $\text{CH}_2\text{Cl}_2$  molecules. Its asymmetric unit features one-quarter of the  $[\text{Tb}^{\text{III}}(\text{O}_2\text{CBu}^t)_4][12\text{-MC-}_{\text{Mn}(\text{III})\text{N}(\text{shi})^{-4}}]^-$  anion, with the  $C_4$  axis passing through the central  $\text{Tb}^{\text{III}}$  ion. There are two isomers in the structure and only the main part will be discussed. Selected interatomic distances and angles for all complexes are listed in Tables S2 and S3. The core of **2** comprises four  $\text{Mn}^{\text{III}}$  and one  $\text{Tb}^{\text{III}}$  atoms arranged in a square pyramidal-like topology with the  $\text{Tb}$  atom occupying the apical position of the pyramid and the  $\text{Mn}$  atoms completing the base (Figure S1).

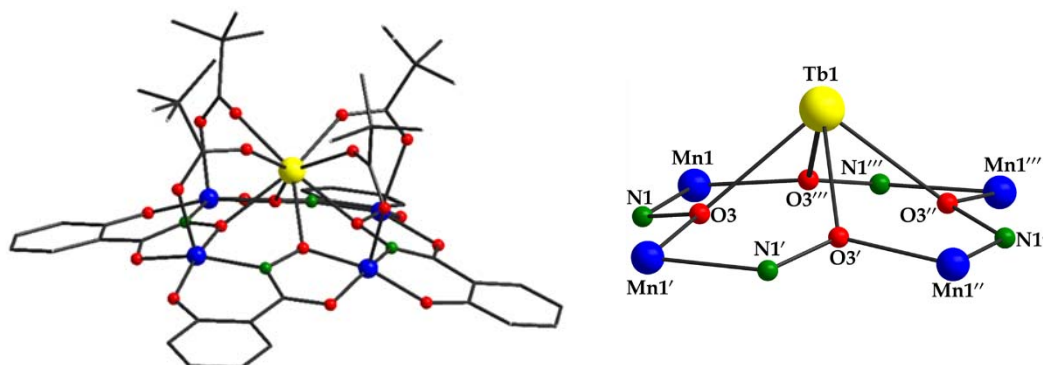


**Figure 1.** Schematic representation of molecular structure and labeled schematic representation of the core  $\{\text{Mn}_4^{\text{III}}\text{Ln}^{\text{III}}(\mu\text{-NO})_4\}^{11+}$  of complex **2**. Color scheme:  $\text{Tb}$ , yellow;  $\text{Mn}^{\text{III}}$ , blue; N, green; O, red. H atoms are omitted for clarity.

The basal  $\text{Mn}^{\text{III}}$  atoms are bridged by diatomic oximate bridges provided by the  $\text{shi}^{3-}$  ligand, giving a  $\text{Mn}\cdots\text{Mn}$  separation of 4.642(9) Å. Note that the coordinated anion of  $\text{shi}^{3-}$  was generated in situ from the metal ion-assisted transformation of  $\text{shaH}_2$  under basic conditions. The large  $\text{Mn-N-O-Mn}$  torsion angle ( $173.3(4)^\circ$ ), which is very close to the ideal linearity of  $180^\circ$ , is responsible for the approximately ideal planarity of the  $\text{Mn}_4$  assembly, whilst the  $\text{Tb}^{\text{III}}$  atom lies 1.789(8) Å out of the  $\text{Mn}_4$  plane. The connection between the basal  $\text{Mn}^{\text{III}}$  and the  $\text{Tb}^{\text{III}}$  atoms is provided by the oximate O atoms of the  $\text{shi}^{3-}$  ligand resulting in a  $\text{Mn}\cdots\text{Tb}$  separation of 3.739(2) Å. Further ligation is provided by four  $\eta^1:\eta^1:\mu$  bridging pivalate ions (Figure 1). The coordination sphere around the  $\text{Mn}$  atoms is completed by the alkoxido and phenoxido O atoms provided by the organic moiety which possesses a  $\eta^1:\eta^1:\eta^1:\eta^2:\mu_3$  coordination mode leading to an overall inorganic core of  $\{\text{Mn}_4^{\text{III}}\text{Ln}^{\text{III}}(\mu\text{-NO})_4\}^{11+}$  (Figure S1).

All  $\text{Mn}^{\text{III}}$  ions are five-coordinate with almost perfect square pyramidal geometry. This has been confirmed by the analysis of the shape-determining bonds and angles using the Reedijk and Addison et al. method [33], which gives us a trigonality index,  $\tau$ , of 0.11 for the four  $\text{Mn}^{\text{III}}$  ions.

The  $\tau = 0.1$  value is consistent with a square pyramidal geometry, as for a perfect square pyramidal geometry a  $\tau$  value of 0 is expected, while a  $\tau$  value of 1 is consistent for a trigonal bipyramidal geometry. The oxidation states of Mn atoms were established by charge balance considerations, metric parameters and bond-valence sum (BVS) calculations [34], with the last providing us with a value of 3.03 for Mn1. Note that the oxidation of  $\text{Mn}^{\text{II}}$  to  $\text{Mn}^{\text{III}}$  occurs undoubtedly by the atmospheric  $\text{O}_2$  under the prevailing basic conditions [35,36]. The central lanthanide ion is eight-coordinate possessing a slightly distorted square antiprismatic geometry with a continuous shape measurement factor of  $\text{CShM} = 0.71$  (Figure S2) [37]. The closest this number is to zero, the closest is the geometry of the lanthanide to the ideal one. Finally, the crystal packing of complex **2** (Figure S2) has revealed that the ionic compounds do not communicate with each other (well separated) in the crystal by any means such as hydrogen bonding or  $\pi$ - $\pi$  stacking interactions but are solely surrounded by the tetrabutylammonium cations and the solvate molecules in the lattice.

Several pivotal geometrical parameters were obtained for complex **2** in order to gain a better understanding of the inner coordination sphere around the lanthanide ion (Figure 2). To be more descriptive, the angle between the four-fold axis and the Ln–O bond direction,  $\theta$ , corresponds to compression or elongation along the tetragonal axis, depending on its value. The magic value for perfect square-antiprismatic (SAP) geometry is  $\theta = 54.74^\circ$ , while smaller angles correspond to elongation and wider ones lead to compression [38–40]. In complex **2**, the average value of  $\theta$  was found to be  $56.15^\circ$ , indicating axial compression. The distance between the upper and lower  $\text{O}_4$ -planes, interplanar distance (dpp), was found to be  $2.639(0) \text{ \AA}$ , while the distances  $d_1$  and  $d_2$  were found to be  $1.103(4) \text{ \AA}$  and  $1.535(6) \text{ \AA}$ , counting for the plane spanned by the carboxylate oxygen atom ( $\text{O}_5$ ) and the one by the oximate oxygen ( $\text{O}_3$ ), respectively. The symmetry of lanthanide's coordination geometry can be further described by another important parameter which is called skew or twist angle. This is the  $\varphi$  angle which basically defines the angle between the diagonals of the two  $\text{O}_4$ -planes. This is a vital parameter for the determination of point group symmetry at the lanthanide site, which consequently leads to assisting on the description of the crystal field substrate composition of lanthanide complexes. When  $\varphi = 0^\circ$  an ideal square prismatic geometry is expected, while when  $\varphi = 45^\circ$  an ideal square antiprismatic geometry is observed. In complex **2** an average  $\varphi$  value of  $43.28(4)^\circ$  was calculated, further supporting the square antiprismatic geometry of the  $\text{Tb}^{\text{III}}$  ion.

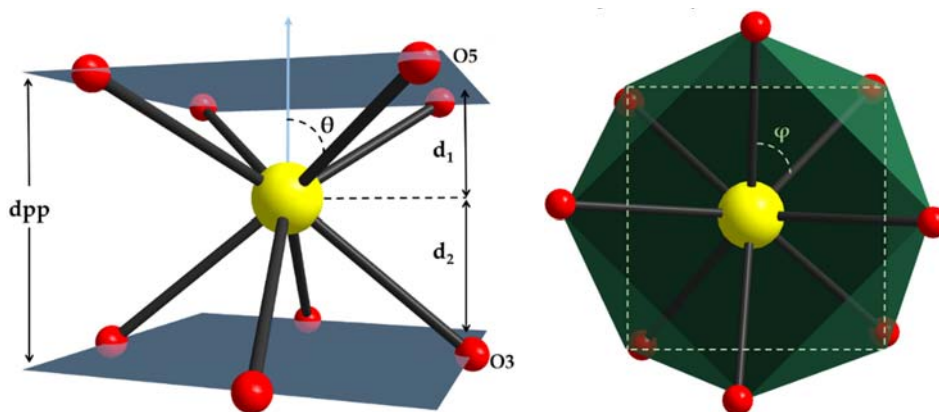


**Figure 2.** Details of structural parameters discussed in the text for complex **2**. Yellow ball: terbium, red ball: oxygen.

## 2.2. Magnetic Studies of Complexes 1–3

Solid state, direct-current (dc) magnetic susceptibility ( $\chi_M$ ) measurements were collected in the temperature range of 2.0–300 K for freshly prepared crystalline samples of **1**, **2**, and **3**, under an applied field of 0.1 T. The obtained data are presented as a  $\chi_M T$  vs.  $T$  plot in Figure 3. The experimental values at 300 K for all complexes ( $18.1 \text{ cm}^3 \cdot \text{mol}^{-1} \cdot \text{K}$  for **1**,  $21.1 \text{ cm}^3 \cdot \text{mol}^{-1} \cdot \text{K}$  for **2** and  $11.4 \text{ cm}^3 \cdot \text{mol}^{-1} \cdot \text{K}$

for **3**) are lower than the theoretical ones ( $19.88 \text{ cm}^3 \cdot \text{mol}^{-1} \cdot \text{K}$  for **1**,  $23.82 \text{ cm}^3 \cdot \text{mol}^{-1} \cdot \text{K}$  for **2** and  $12.0 \text{ cm}^3 \cdot \text{mol}^{-1} \cdot \text{K}$  for **3**) expected for four non-interacting  $\text{Mn}^{\text{III}}$  ions ( $S = 2$ ,  $g = 2$ ) and one  $\text{Gd}^{\text{III}}$  ( ${}^8\text{S}_{7/2}$ ,  $S = 7/2$ ,  $L = 0$ ,  $g = 2$ ), one  $\text{Tb}^{\text{III}}$  ( ${}^7\text{F}_6$ ,  $S = 3$ ,  $L = 3$ ,  $g = 3/2$ ), or one diamagnetic  $\text{Y}^{\text{III}}$  ion [41]. All complexes possess a similar magnetic behavior, with the  $\chi_{\text{M}}T$  steadily decreasing with decreasing temperature from 300 K till 2 K, where it reaches values of  $6.95 \text{ cm}^3 \cdot \text{K} \cdot \text{mol}^{-1}$  for **1**,  $3.30 \text{ cm}^3 \cdot \text{K} \cdot \text{mol}^{-1}$  for **2** and  $0.2 \text{ cm}^3 \cdot \text{K} \cdot \text{mol}^{-1}$  for **3**, respectively. The shape of the  $\chi_{\text{M}}T$  vs.  $T$  plots for all complexes indicates the presence of predominant antiferromagnetic exchange interactions within the metal centers. This is further supported by the fact that the  $\chi_{\text{M}}T$  values at 300 K for all complexes are lower than the expected theoretical ones.

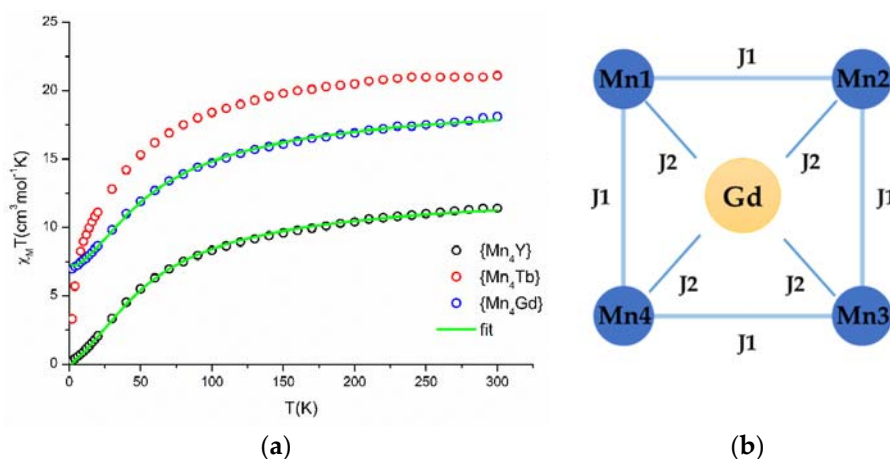


**Figure 3.** (a) Temperature dependence of magnetic susceptibility for complexes **1**, **2**, and **3**. Green solid line represents simulation of the data in complexes **1** and **3**; see text for details and fitting parameters. (b) Fitting model for complex **1**.

In order to gain better insight in the strength of the intramolecular  $\text{Mn}^{\text{III}}\text{--Mn}^{\text{III}}$  magnetic exchange interactions, the magnetic susceptibility data of complex **3** were fit using PHI [42] program. The magnetic susceptibility data of complex **3**, which comprises the diamagnetic  $\text{Y}^{\text{III}}$  ion in the central cavity, were fit using a  $1\text{-}J$  model according to the spin Hamiltonian:

$$\hat{H} = -2J (\hat{S}_{\text{Mn1}} \cdot \hat{S}_{\text{Mn2}} + \hat{S}_{\text{Mn2}} \cdot \hat{S}_{\text{Mn3}} + \hat{S}_{\text{Mn3}} \cdot \hat{S}_{\text{Mn4}} + \hat{S}_{\text{Mn4}} \cdot \hat{S}_{\text{Mn1}})$$

An excellent simulation of the data (solid green line, Figure 3) was achieved with a  $J = -3.74 \text{ cm}^{-1}$  and  $g = 2.07$ . The antiferromagnetic exchange interactions are anticipated for a system that is exclusively coupled via oximate bridges that give very large  $\text{Mn}\text{--N}\text{--O}\text{--Mn}$  torsion angles, which are known to promote antiferromagnetic exchange interactions [43].

In order to also quantify the nature of the  $\text{Mn}^{\text{III}}\text{--Ln}^{\text{III}}$  exchange interactions, complex **1** was also fit, using a  $2\text{-}J$  model, which counts for the outer  $\text{Mn}^{\text{III}}\text{--Mn}^{\text{III}}$  ( $J_1$ ) interactions as well as for inner the  $\text{Mn}^{\text{III}}\text{--Gd}^{\text{III}}$  ( $J_2$ ) interaction, shown in Figure 3b. The data were fit according to the spin Hamiltonian shown below:

$$\hat{H} = -2J_1 (\hat{S}_{\text{Mn1}} \cdot \hat{S}_{\text{Mn2}} + \hat{S}_{\text{Mn2}} \cdot \hat{S}_{\text{Mn3}} + \hat{S}_{\text{Mn3}} \cdot \hat{S}_{\text{Mn4}} + \hat{S}_{\text{Mn4}} \cdot \hat{S}_{\text{Mn1}}) - 2J_2 (\hat{S}_{\text{Mn1}} \cdot \hat{S}_{\text{Gd}} + \hat{S}_{\text{Mn2}} \cdot \hat{S}_{\text{Gd}} + \hat{S}_{\text{Mn3}} \cdot \hat{S}_{\text{Gd}} + \hat{S}_{\text{Mn4}} \cdot \hat{S}_{\text{Gd}})$$

An excellent fit of the data (solid green line, Figure 3) could be obtained with  $J_1 = -3.35 \text{ cm}^{-1}$ ,  $J_2 = -0.45 \text{ cm}^{-1}$  and  $g_{\text{Mn(III)}} = 1.99$ . The values of both models are in an excellent agreement. Note that antiferromagnetic exchange interactions, in  $\text{Mn}^{\text{III}}\text{--Gd}^{\text{III}}$  and other  $3\text{d}\text{--Gd}^{\text{III}}$  species, possessing the  $3\text{d}_{x^2-y^2}$  orbital unoccupied, are quite often observed [44–47]. Here is the first time that fitting of the magnetic susceptibility data for  $3\text{d}/\text{Gd}^{\text{III}}$  interactions has been reported, within the MC family of complexes.

Field-dependent magnetization measurements were also performed for complexes **1** and **2** at temperatures between 2 K and 10 K over the range of 0–7 T (Figure 4 and Figure S8). The magnetization of **1** and **2** shows a rapid increase below 1 T followed by a slow, nearly linear increase without reaching saturation. The lack of saturation in magnetization of **1** and **2** indicates the presence of magnetic anisotropy and/or population of the Ln<sup>III</sup> low-lying excited states, as well as the effect from some weak antiferromagnetic components between the metal centers.

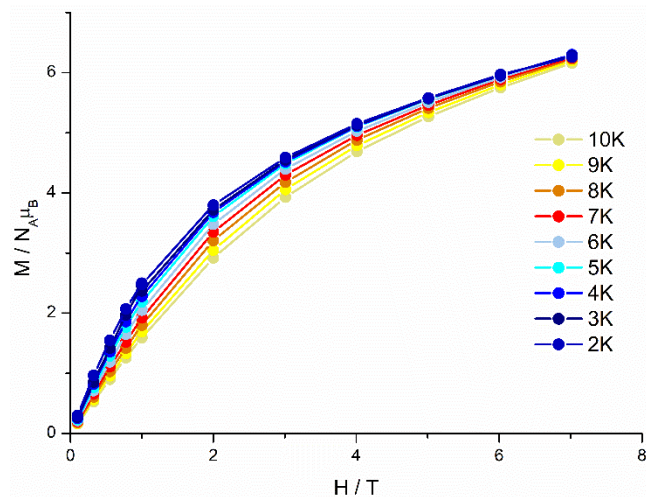


**Figure 4.** (a) Temperature dependence of magnetic susceptibility for complexes **1**, **2**, and **3**. Green solid line represents simulation of the data in complexes **1** and **3**; see text for details and fitting parameters. (b) Fitting model for complex **1**.

### 3. Materials and Methods

#### 3.1. General Information

All chemicals and solvents used for synthesis were of reagent grade and used as purchased without further purification. The starting material  $\text{Mn}(\text{O}_2\text{CBu}^t)_2 \cdot 2\text{H}_2\text{O}$  was synthesized using literature procedures [48]. C, H and N elemental analyses were carried out on a Foss Heraeus Vario EL (Elementar Analysensysteme GmbH, Langenselbold, Germany) at the Institute of Organic Chemistry at the Johannes Gutenberg University Mainz. Infrared absorption spectra were recorded at room temperature in a range of  $3000\text{--}400\text{ cm}^{-1}$  on a Thermo Fischer NICOLET Nexus FT/IR-5700 spectrometer (Thermo Fischer Scientific, Waltham, MA, USA) equipped with Smart Orbit ATR Diamond cell (Thermo Fischer Scientific, Waltham, MA, USA). UV–Vis absorption measurements were performed between for complexes **1**, **2** and **3** in MeCN between 200 nm and 1000 nm on a JASCO V-570 UV/Vis/NIR spectrophotometer (JASCO Inc., Easton, MD, USA) (Figure S7 in Supplementary Materials).

A similar procedure has been used to isolate compounds **1–3**.

$(^t\text{Bu}_4\text{N})\{[\text{Gd}^{\text{III}}(\text{O}_2\text{CBu}^t)_4][12\text{-MC-Mn(III)N}(\text{shi})\text{-4}]\} \cdot 5\text{CH}_2\text{Cl}_2$  (**1**· $5\text{CH}_2\text{Cl}_2$ ): To an almost colorless solution of shiH<sub>3</sub> (30.50 mg, 0.2 mmol) and morpholine (18  $\mu\text{L}$ , 0.2 mmol) in  $\text{CH}_2\text{Cl}_2$  was added  $\text{Mn}(\text{O}_2\text{CBu}^t)_2 \cdot 2\text{H}_2\text{O}$  (55.00 mg, 0.2 mmol) followed by stirring for 5 min. To the resulting dark brown almost clear solution  $\text{Gd}(\text{NO}_3)_3 \cdot \text{H}_2\text{O}$  (6.00 mg, 0.025 mmol) was added along with  $^t\text{Bu}_4\text{NClO}_4$  (26.00 mg, 0.075 mmol) and left for stirring for another 40 min. The solution was subsequently filtered and left for crystallization. Layering hexane gave diffraction quality crystals of **1**· $5\text{CH}_2\text{Cl}_2$  after 5 days which were collected by filtration, washed with hexanes ( $3 \times 5\text{ mL}$ ) and dried in air. Yield: 0.032 g (59%) based on the Gd<sup>III</sup> ion. The air-dried solid was analyzed as (**1**): C, 47.32; H, 5.46; N, 4.3. Found: C, 47.44; H, 5.49; N, 4.38. Selected ATR data ( $\text{cm}^{-1}$ ): 2961 (w), 2292 (w), 2875 (w), 1598 (w), 1569 (s), 1538 (w), 1421 (w), 1096 (m), 867 (w), 768 (w), 683 (s), 649 (w), 617 (m), 482 (m).

(<sup>t</sup>Bu<sub>4</sub>N){[Tb<sup>III</sup>(O<sub>2</sub>CBu<sup>t</sup>)<sub>4</sub>][12-MC-Mn(III)N(Shi)-4]}·5CH<sub>2</sub>Cl<sub>2</sub> (2·5CH<sub>2</sub>Cl<sub>2</sub>): Compound 2·5CH<sub>2</sub>Cl<sub>2</sub> was synthesized with the similar procedure as compound 1·5CH<sub>2</sub>Cl<sub>2</sub>, except that Tb(NO<sub>3</sub>)<sub>3</sub>·H<sub>2</sub>O (8.50 mg, 0.025 mmol) was used instead of Gd(NO<sub>3</sub>)<sub>3</sub>·H<sub>2</sub>O. Yield: 0.039 g (76%) based on the Tb<sup>III</sup> ion. The air-dried solid was analyzed as (2): C, 47.27; H, 5.46; N, 4.31. Found: C, 47.38; H, 5.52; N, 4.34. Selected ATR data (cm<sup>-1</sup>): 2961 (w), 2929 (w), 2874 (w), 1597 (w), 1568 (s), 1537 (w), 1421 (w), 1099 (m), 865 (w), 771 (w), 721 (s), 649 (w), 683 (s), 600 (m), 482 (m).

(<sup>t</sup>Bu<sub>4</sub>N)<sub>2</sub>{[Y<sup>III</sup>(O<sub>2</sub>CBu<sup>t</sup>)<sub>4</sub>][12-MC-Mn(III)N(Shi)-4]}·(ClO<sub>4</sub>) (3): Compound 3 was synthesized with the similar procedure as compounds 1 and 2, except that this time Y(NO<sub>3</sub>)<sub>3</sub>·H<sub>2</sub>O (0.01 mg, 0.025 mmol) was used. Yield: 0.028 g (59%) based on the Y<sup>III</sup> ion. The air-dried solid was analyzed as (3): C, 50.63; H, 6.59; N, 4.43. Found: C, 50.74; H, 6.71; N, 4.51. Selected ATR data (cm<sup>-1</sup>): 2961 (w), 2929 (w), 2874 (w), 1596 (w), 1569 (m), 1424 (w), 1099 (m), 865 (w), 771 (w), 684 (s), 649 (w), 600 (m), 482 (m).

### 3.2. X-ray Crystallography

X-ray diffraction data for the structure analysis were collected from suitable single crystals on a Bruker SMART with an APEX II CCD detector (1, 2) (Bruker AXS GmbH, Karlsruhe, Germany) and on a STOE IPDS 2 T (3) (STOE & Cie GmbH, Darmstadt, Germany) equipped with an Oxford cooling system (Oxford Cryosystems Ltd., Oxford, UK) operating at 173(2) K (1, 2) and at 120(2)K (3), respectively. Graphite-monochromated Mo-K $\alpha$  radiation ( $\lambda = 0.71073 \text{ \AA}$ ) from long-fine focus sealed X-ray tube was used throughout. Data reduction and absorption correction were done with *Bruker Apex v3.0* [49,50] and *SADABS*[ $\times 11$ ] (1, 2) or with *STOE X-RED* [51] (3). Structures were solved with *SHELXT* [52] and refined by full-matrix least-squares on F-squared using *SHELXL* [53], interfaced through *Olex2* [54]. All non-hydrogen atoms were refined with anisotropic displacement parameters, while all hydrogen atoms have been placed on idealized positions using a riding model. In complexes 1, 2 and 3 the anionic (metallacrown) part show isomerism and are disordered over two positions. The metallacrowns can be arranged clockwise [M–NO–M] or anticlockwise [M–ON–M], with slightly different position for the transition metal ions, while the central lanthanide ion remains on its position in both isomers. The site occupation factor of the isomers were refined free to 0.82/0.18, 0.80/0.20 and 0.91/0.09 for 1, 2 and 3, respectively. While in 1 and 2 the whole anionic part was refined over two positions, in 3 only the manganese ions were refined over two positions, due to the low occupancy of the second isomer. The cationic counter ions Bu<sub>4</sub>N<sup>+</sup> were refined over two positions with a fixed ratio of 0.6/0.4 in 1 and 2. CCDC 1849727–1849729 (1–3) contains the supplementary crystallographic data for the structure reported in this paper.

### 3.3. Magnetic Measurements

Variable-temperature direct current (dc) magnetic susceptibility measurements were performed on polycrystalline samples with the use of Quantum Design SQUID magnetometer MPMS-7 equipped with a 7 T magnet. The samples were embedded in eicosane to avoid orientation of the crystallites under the applied field. Experimental susceptibility data were corrected for the underlying diamagnetism using Pascal's constants [55]. The temperature dependent magnetic contribution of the holder and of the embedding matrix eicosane were experimentally determined and subtracted from the measured susceptibility data. Variable temperature susceptibility data were collected in a temperature range of 2–300 K under an applied field of 0.1 Tesla, while magnetization data were collected between 2 K and 10 K and magnetic fields up to 7 Tesla. Alternating-current (ac) measurements were performed with an oscillating magnetic field of 3 Oe at frequencies ranging from 1 Hz to 1400 Hz.

## 4. Conclusions

In summary, we reported a new family of Mn<sup>III</sup>/Ln<sup>III</sup> 12-MC-4 complexes, derived from the reaction of Mn(O<sub>2</sub>CBu<sup>t</sup>)<sub>2</sub>·2H<sub>2</sub>O with various nitrate salts of lanthanides in the presence of salicylhydroxamic acid. Direct-current (dc) magnetic susceptibility studies revealed the presence

of antiferromagnetic exchange interactions between the metal centers, while fitting of the data using the  $\{Mn_4Y\}$  complex allowed us to quantify the strength of the interactions within the outer  $Mn^{III}$  ions, which was found to be  $J = -3.74 \text{ cm}^{-1}$  with  $g = 2.07$ . Moreover, fitting of the  $\{Mn_4Gd\}$  (1) data gave an extra insight into the strength of the magnetic exchange interactions, especially for the  $Mn^{III}-Gd^{III}$  intramolecular interaction, revealing values of  $J_{Mn-Mn} = -3.35 \text{ cm}^{-1}$ ,  $J_{Mn-Gd} = -0.45 \text{ cm}^{-1}$  and  $g_{Mn(III)} = 1.99$ . Note that this is the first example within the family of metallacrowns (MCs), where simulation of the magnetic data has been reported. In-phase and out-of-phase (ac) magnetic susceptibility measurements as a function of temperature did not reveal any slow relaxation in fields of  $H_{dc} = 0-3000 \text{ Oe}$ . In order to further improve the magnetic properties of such compounds, the chemistry will be broadened to the use of other magnetic or diamagnetic  $3d$  and  $4f$  metal ions, by means of modifying the structural and/or physical properties of the resulting molecular compounds.

**Supplementary Materials:** Supplementary materials are available online at <http://www.mdpi.com/2304-6740/6/3/66/s1>, CIF and checkCIF files of compounds 1, 2 and 3, Figure S1: Coordination modes of ligands in complex 2, Figure S2: Labeled schematic representation of the core  $\{Mn_4^{III}Ln^{III}(\mu-NO)_4\}^{11+}$  of complex 2. Color scheme: Tb, yellow;  $Mn^{III}$ , blue; N, green; O, red, Figure S3: Crystal packing representation in complex 2, Figure S4: IR spectrum for complex 1, Figure S5: IR spectrum for complex 2, Figure S6: IR spectrum for complex 3, Figure S7: UV-Vis spectra of 1 (black), 2 (red), 3 (blue), and  $shH_3$  (green) in MeCN, Figure S8:  $M$  vs.  $H$  plots for complex 1 in various temperatures as indicated. Solid lines are guidelines for the eyes, Table S1: Crystallographic data for complexes 1–3, Table S2: Selected bond lengths for complex 2, Table S3: Selected Bond Angles for 2, Table S4: Shape measurements of the 8-coordinate lanthanide coordination polyhedra. The bold numbers indicate the closest polyhedron according to SHAPE calculations.

**Author Contributions:** A.A.A. designed and performed the experiments. She analyzed most of the data and wrote the paper. L.M.C. refined the structures and helped a lot with his knowledgeable input throughout the paper-writing process. E.R. was involved during the writing of the paper to every step of the process giving valuable feedback.

**Funding:** This research received no external funding.

**Acknowledgments:** We are very grateful to Regine Jung-Pothmann and Dieter Schollmeyer for the collection of the X-ray diffraction data of all our complexes. Angeliki A. Athanasopoulou is a member of (SFB/TRR) 173 “Spin+X-Spin its collective environment” and a fellow of the Excellence Initiative by the Graduate School Materials Science in Mainz, Germany (DFG/GSC 266), both initiated by the Deutsche Forschungsgemeinschaft (DFG, GermanResearchFoundation).

**Conflicts of Interest:** The authors declare no conflict of interest.

## References

1. Chow, C.Y.; Trivedi, E.R.; Pecoraro, V.; Zaleski, C.M. Heterometallic Mixed  $3d-4f$  Metallacrowns: Structural Versatility, Luminescence, and Molecular Magnetism. *Comments Inorg. Chem.* **2015**, *35*, 214–253. [[CrossRef](#)]
2. Jia, R.; Li, H.-F.; Chen, P.; Gao, T.; Sun, W.-B.; Li, G.-M.; Yan, P.-F. Synthesis, Structure, and Tunable White Light Emission of Heteronuclear  $Zn_2 Ln_2$  Arrays Using a Zinc Complex as Ligand. *CrystEngComm* **2016**, *18*, 917–923. [[CrossRef](#)]
3. Evangelisti, F.; Moré, R.; Hodel, F.; Lubber, S.; Patzke, G.R.  $3d-4f$   $\{Co^{II}_3Ln(OR)_4\}$  Cubanes as Bio-Inspired Water Oxidation Catalysts. *J. Am. Chem. Soc.* **2015**, *137*, 11076–11084. [[CrossRef](#)] [[PubMed](#)]
4. Rosado Piquer, L.; Sañudo, E.C. Heterometallic  $3d-4f$  Single-Molecule Magnets. *Dalton Trans.* **2015**, *44*, 8771–8780. [[CrossRef](#)] [[PubMed](#)]
5. Woodruff, D.N.; Winpenny, R.E.P.; Layfield, R.A. Lanthanide Single-Molecule Magnets. *Chem. Rev.* **2013**, *113*, 5110–5148. [[CrossRef](#)] [[PubMed](#)]
6. Christou, G.; Gatteschi, D.; Hendrickson, D.N.; Sessoli, R. Single-Molecule Magnets. *MRS Bull.* **2000**, *25*, 66–71. [[CrossRef](#)]
7. Bagai, R.; Christou, G. The Drosophila of Single-Molecule Magnetism:  $[Mn_{12}O_{12}(O_2CR)_{16}(H_2O)_4]$ . *Chem. Soc. Rev.* **2009**, *38*, 1011. [[CrossRef](#)] [[PubMed](#)]
8. Friedman, J.R.; Sarachik, M.P.; Tejada, J.; Ziolo, R. Macroscopic Measurement of Resonant Magnetization Tunneling in High-Spin Molecules. *Phys. Rev. Lett.* **1996**, *76*, 3830–3833. [[CrossRef](#)] [[PubMed](#)]
9. Thomas, L.; Lionti, F.; Ballou, R.; Gatteschi, D.; Sessoli, R.; Barbara, B. Macroscopic Quantum Tunneling of Magnetization in a Single Crystal of Nanomagnets. *Nature* **1996**, *383*, 145–147. [[CrossRef](#)]

10. Bogani, L.; Wernsdorfer, W. Molecular Spintronics Using Single-Molecule Magnets. *Nat. Mater.* **2008**, *7*, 179–186. [[CrossRef](#)] [[PubMed](#)]
11. Urdampilleta, M.; Klyatskaya, S.; Cleuziou, J.-P.; Ruben, M.; Wernsdorfer, W. Supramolecular Spin Valves. *Nat. Mater.* **2011**, *10*, 502–506. [[CrossRef](#)] [[PubMed](#)]
12. Lah, M.S.; Kirk, M.L.; Hatfield, W.; Pecoraro, V.L. The Tetranuclear Cluster  $\text{Fe}^{\text{III}}[\text{Fe}^{\text{III}}(\text{Salicylhydroximato})(\text{MeOH})(\text{Acetate})_3]$  Is an Analogue of  $\text{M}^{3+}(9\text{-Crown-3})$ . *J. Chem. Soc. Chem. Commun.* **1989**, 1606–1608. [[CrossRef](#)]
13. Lah, M.S.; Pecoraro, V.L. Isolation and Characterization of  $\{\text{Mn}^{\text{II}}[\text{Mn}^{\text{III}}(\text{Salicylhydroximate})_4(\text{Acetate})_2(\text{DMF})_6\} \cdot 2\text{DMF}$ : An Inorganic Analog of  $\text{M}^{2+}(12\text{-Crown-4})$ . *J. Am. Chem. Soc.* **1989**, *111*, 7258–7259. [[CrossRef](#)]
14. Dutton, J.C.; Murray, K.S.; Tiekink, E.R.T. Magnetism of Oxovanadium(IV) Complexes of Binucleating Ligands. Oxidation to and Structure of a Mononuclear Oxovanadium(V) Complex of  $N,N'$ -(Pentan-3-Ol) Bis(Salicylaldimine). *Inorg. Chim. Acta* **1989**, *166*, 5–8. [[CrossRef](#)]
15. Mezei, G.; Zaleski, C.M.; Pecoraro, V.L. Structural and Functional Evolution of Metallacrowns. *Chem. Rev.* **2007**, *107*, 4933–5003. [[CrossRef](#)] [[PubMed](#)]
16. Tegoni, M.; Furlotti, M.; Tropiano, M.; Lim, C.S.; Pecoraro, V.L. Thermodynamics of Core Metal Replacement and Self-Assembly of  $\text{Ca}^{2+}$  15-Metallacrown-5<sup>+</sup>. *Inorg. Chem.* **2010**, *49*, 5190–5201. [[CrossRef](#)] [[PubMed](#)]
17. Jones, L.F.; Kilner, C.A.; Halcrow, M.A. A Cobalt Metallacrown Anion Host with Guest-Dependent Redox Activity. *Chem. Eur. J.* **2009**, *15*, 4667–4675. [[CrossRef](#)] [[PubMed](#)]
18. Jones, L.F.; Barrett, S.A.; Kilner, C.A.; Halcrow, M.A. Ammonium, Alkylammonium, and Amino Acid Complexes of a Hexacopper Fluoro-Metallacrown Cavitand. *Chem. Eur. J.* **2008**, *14*, 223–233. [[CrossRef](#)] [[PubMed](#)]
19. Chow, C.Y.; Eliseeva, S.V.; Trivedi, E.R.; Nguyen, T.N.; Kampf, J.W.; Petoud, S.; Pecoraro, V.L.  $\text{Ga}^{3+}/\text{Ln}^{3+}$  Metallacrowns: A Promising Family of Highly Luminescent Lanthanide Complexes That Covers Visible and Near-Infrared Domains. *J. Am. Chem. Soc.* **2016**, *138*, 5100–5109. [[CrossRef](#)] [[PubMed](#)]
20. Trivedi, E.R.; Eliseeva, S.V.; Jankolovits, J.; Olmstead, M.M.; Petoud, S.; Pecoraro, V.L. Highly Emitting Near-Infrared Lanthanide “Encapsulated Sandwich” Metallacrown Complexes with Excitation Shifted Toward Lower Energy. *J. Am. Chem. Soc.* **2014**, *136*, 1526–1534. [[CrossRef](#)] [[PubMed](#)]
21. Ostrowska, M.; Fritsky, I.O.; Gumienna-Kontecka, E.; Pavlishchuk, A.V. Metallacrown-Based Compounds: Applications in Catalysis, Luminescence, Molecular Magnetism, and Adsorption. *Coord. Chem. Rev.* **2016**, 327–328, 304–332. [[CrossRef](#)]
22. Athanasopoulou, A.A.; Gamer, C.; Völker, L.; Rentschler, E. *Novel Magnetic Nanostructures: Unique Properties and Applications*; ELSEVIER: New York, NY, USA, 2018.
23. Qin, Y.; Gao, Q.; Chen, Y.; Liu, W.; Lin, F.; Zhang, X.; Dong, Y.; Li, Y. Four Mixed 3d-4f 12-Metallacrown-4 Complexes: Syntheses, Structures and Magnetic Properties. *J. Clust. Sci.* **2017**, *28*, 891–903. [[CrossRef](#)]
24. Cao, F.; Wang, S.; Li, D.; Zeng, S.; Niu, M.; Song, Y.; Dou, J. Family of Mixed 3d-4f Dimeric 14-Metallacrown-5 Compounds: Syntheses, Structures, and Magnetic Properties. *Inorg. Chem.* **2013**, *52*, 10747–10755. [[CrossRef](#)] [[PubMed](#)]
25. Lou, T.; Yang, H.; Zeng, S.; Li, D.; Dou, J. A New Family of Heterometallic  $\text{LnIII}[12\text{-MCFeIIIN}(\text{Shi})\text{-4}]$  Complexes: Syntheses, Structures and Magnetic Properties. *Crystals* **2018**, *8*, 229. [[CrossRef](#)]
26. Azar, M.R.; Boron, T.T.; Lutter, J.C.; Daly, C.I.; Zegalia, K.A.; Nimthong, R.; Ferrence, G.M.; Zeller, M.; Kampf, J.W.; Pecoraro, V.L.; et al. Controllable Formation of Heterotrimetallic Coordination Compounds: Systematically Incorporating Lanthanide and Alkali Metal Ions into the Manganese 12-Metallacrown-4 Framework. *Inorg. Chem.* **2014**, *53*, 1729–1742. [[CrossRef](#)] [[PubMed](#)]
27. Travis, J.R.; Zeller, M.; Zaleski, C.M. Facile Carboxylate Ligand Variation of Heterotrimetallic 12-Metallacrown-4 Complexes. *Polyhedron* **2016**, *114*, 29–36. [[CrossRef](#)]
28. Boron, T.T.; Lutter, J.C.; Daly, C.I.; Chow, C.Y.; Davis, A.H.; Nimthong-Roldán, A.; Zeller, M.; Kampf, J.W.; Zaleski, C.M.; Pecoraro, V.L. The Nature of the Bridging Anion Controls the Single-Molecule Magnetic Properties of  $\text{DyX}_4\text{M}$  12-Metallacrown-4 Complexes. *Inorg. Chem.* **2016**, *55*, 10597–10607. [[CrossRef](#)] [[PubMed](#)]
29. Happ, P.; Rentschler, E. Enforcement of a High-Spin Ground State for the First 3d Heterometallic 12-Metallacrown-4 Complex. *Dalton Trans.* **2014**, 43, 15308–15312. [[CrossRef](#)] [[PubMed](#)]
30. Happ, P.; Plenck, C.; Rentschler, E. 12-MC-4 Metallacrowns as Versatile Tools for SMM Research. *Coord. Chem. Rev.* **2015**, 289–290, 238–260. [[CrossRef](#)]

31. Plenck, C.; Krause, J.; Beck, M.; Rentschler, E. Rational Linkage of Magnetic Molecules Using Click Chemistry. *Chem. Commun.* **2015**, *51*, 6524–6527. [[CrossRef](#)] [[PubMed](#)]
32. Happ, P.; Sapozhnik, A.; Klanke, J.; Czaja, P.; Chernenkaya, A.; Medjanik, K.; Schuppler, S.; Nagel, P.; Merz, M.; Rentschler, E.; et al. Analyzing the Enforcement of a High-Spin Ground State for a Metallocrown Single-Molecule Magnet. *Phys. Rev. B* **2016**, *93*, 174404. [[CrossRef](#)]
33. Addison, A.W.; Rao, T.N.; Reedijk, J.; van Rijn, J.; Verschoor, G.C. Synthesis, Structure, and Spectroscopic Properties of Copper(II) Compounds Containing Nitrogen–sulphur Donor Ligands; the Crystal and Molecular Structure of Aqua[1,7-Bis(*N*-Methylbenzimidazol-2'-yl)-2,6-Dithiaheptane]Copper(II) Perchlorate. *J. Chem. Soc. Dalton Trans.* **1984**, 1349–1356. [[CrossRef](#)]
34. Liu, W.; Thorp, H.H. Bond Valence Sum Analysis of Metal-Ligand Bond Lengths in Metalloenzymes and Model Complexes. 2. Refined Distances and Other Enzymes. *Inorg. Chem.* **1993**, *32*, 4102–4105. [[CrossRef](#)]
35. Alaimo, A.A.; Koumoussi, E.S.; Cunha-Silva, L.; McCormick, L.J.; Teat, S.J.; Psycharis, V.; Raptopoulou, C.P.; Mukherjee, S.; Li, C.; Gupta, S.D.; et al. Structural Diversities in Heterometallic Mn–Ca Cluster Chemistry from the Use of Salicylhydroxamic Acid: {Mn<sup>III</sup><sub>4</sub>Ca<sub>2</sub>}, {Mn<sup>II/III</sup><sub>6</sub>Ca<sub>2</sub>}, {Mn<sup>III/IV</sup><sub>8</sub>Ca}, and {Mn<sup>III</sup><sub>8</sub>Ca<sub>2</sub>} Complexes with Relevance to Both High- and Low-Valent States of the Oxygen-Evolving Complex. *Inorg. Chem.* **2017**, *56*, 10760–10774. [[CrossRef](#)] [[PubMed](#)]
36. Stoumpos, C.C.; Gass, I.A.; Milios, C.J.; Lalioti, N.; Terzis, A.; Aromí, G.; Teat, S.J.; Brechin, E.K.; Perlepes, S.P. A Mn<sup>II</sup><sub>4</sub> Cubane and a Novel Mn<sup>II</sup><sub>10</sub>Mn<sup>III</sup><sub>4</sub> Cluster from the Use of Di-2-Pyridyl Ketone in Manganese Acetate Chemistry. *Dalton Trans.* **2009**, 307–317. [[CrossRef](#)] [[PubMed](#)]
37. Alvarez, S.; Alemany, P.; Casanova, D.; Cirera, J.; Llunell, M.; Avnir, D. Shape Maps and Polyhedral Interconversion Paths in Transition Metal Chemistry. *Coord. Chem. Rev.* **2005**, *249*, 1693–1708. [[CrossRef](#)]
38. Sorace, L.; Benelli, C.; Gatteschi, D. Lanthanides in Molecular Magnetism: Old Tools in a New Field. *Chem. Soc. Rev.* **2011**, *40*, 3092. [[CrossRef](#)] [[PubMed](#)]
39. Baldoví, J.J.; Cardona-Serra, S.; Clemente-Juan, J.M.; Coronado, E.; Gaita-Ariño, A.; Palií, A. Rational Design of Single-Ion Magnets and Spin Qubits Based on Mononuclear Lanthanoid Complexes. *Inorg. Chem.* **2012**, *51*, 12565–12574. [[CrossRef](#)] [[PubMed](#)]
40. Sørensen, M.A.; Weihe, H.; Vinum, M.G.; Mortensen, J.S.; Doerrer, L.H.; Bendix, J. Imposing High-Symmetry and Tuneable Geometry on Lanthanide Centres with Chelating Pt and Pd Metalloligands. *Chem. Sci.* **2017**, *8*, 3566–3575. [[CrossRef](#)]
41. Benelli, C.; Gatteschi, D. Magnetism of Lanthanides in Molecular Materials with Transition-Metal Ions and Organic Radicals. *Chem. Rev.* **2002**, *102*, 2369–2388. [[CrossRef](#)] [[PubMed](#)]
42. Chilton, N.F.; Anderson, R.P.; Turner, L.D.; Soncini, A.; Murray, K.S. PHI: A Powerful New Program for the Analysis of Anisotropic Monomeric and Exchange-Coupled Polynuclear *d*- and *f*-Block Complexes. *J. Comput. Chem.* **2013**, *34*, 1164–1175. [[CrossRef](#)] [[PubMed](#)]
43. Milios, C.J.; Piligkos, S.; Brechin, E.K. Ground State Spin-Switching via Targeted Structural Distortion: Twisted Single-Molecule Magnets from Derivatized Salicylaloximes. *Dalton Trans.* **2008**, 1809–1817. [[CrossRef](#)] [[PubMed](#)]
44. Papatriantafyllopoulou, C.; Abboud, K.A.; Christou, G. Carboxylate-Free Mn<sup>III</sup><sub>2</sub>Ln<sup>III</sup><sub>2</sub> (Ln = Lanthanide) and Mn<sup>III</sup><sub>2</sub>Y<sup>III</sup><sub>2</sub> Complexes from the Use of (2-Hydroxymethyl)pyridine: Analysis of Spin Frustration Effects. *Inorg. Chem.* **2011**, *50*, 8959–8966. [[CrossRef](#)] [[PubMed](#)]
45. Savva, M.; Skordi, K.; Fournet, A.D.; Thuijs, A.E.; Christou, G.; Perlepes, S.P.; Papatriantafyllopoulou, C.; Tasiopoulos, A.J. Heterometallic Mn<sup>III</sup><sub>4</sub>Ln<sub>2</sub> (Ln = Dy, Gd, Tb) Cross-Shaped Clusters and Their Homometallic Mn<sup>III</sup><sub>4</sub>Mn<sup>II</sup><sub>2</sub> Analogues. *Inorg. Chem.* **2017**, *56*, 5657–5668. [[CrossRef](#)] [[PubMed](#)]
46. Liu, S.-J.; Xie, X.-R.; Zheng, T.-F.; Bao, J.; Liao, J.-S.; Chen, J.-L.; Wen, H.-R. Three-Dimensional Two-Fold Interpenetrated Cr<sup>III</sup>–Gd<sup>III</sup> Heterometallic Framework as an Attractive Cryogenic Magnetorefrigerant. *CrystEngComm* **2015**, *17*, 7270–7275. [[CrossRef](#)]
47. Gómez, V.; Vendier, L.; Corbella, M.; Costes, J.-P. Tetranuclear [Co–Gd]<sub>2</sub> Complexes: Aiming at a Better Understanding of the 3d–Gd Magnetic Interaction. *Inorg. Chem.* **2012**, *51*, 6396–6404. [[CrossRef](#)] [[PubMed](#)]
48. Yu, S.B.; Lippard, S.J.; Shweky, I.; Bino, A. Dinuclear Manganese(II) Complexes with Water and Carboxylate Bridges. *Inorg. Chem.* **1992**, *31*, 3502–3504. [[CrossRef](#)]
49. Bruker Apex 3; Bruker AXS Inc.: Madison, WI, USA, 2016.
50. Sheldrick, G.M. *SADABS-2016/2*; Bruker AXS Inc.: Madison, WI, USA, 2016.
51. *Stoe & Cie X-RED*; Stoe & Cie: Darmstadt, Germany, 2002.

52. Sheldrick, G.M. *SHELXT*—Integrated Space-Group and Crystal-Structure Determination. *Acta Crystallogr. Sect. Found. Adv.* **2015**, *71*, 3–8. [[CrossRef](#)] [[PubMed](#)]
53. Sheldrick, G.M. Crystal Structure Refinement with *SHELXL*. *Acta Crystallogr. Sect. C Struct. Chem.* **2015**, *71*, 3–8. [[CrossRef](#)] [[PubMed](#)]
54. Dolomanov, O.V.; Bourhis, L.J.; Gildea, R.J.; Howard, J.A.K.; Puschmann, H. *OLEX2*: A Complete Structure Solution, Refinement and Analysis Program. *J. Appl. Crystallogr.* **2009**, *42*, 339–341. [[CrossRef](#)]
55. Bain, G.A.; Berry, J.F. Diamagnetic Corrections and Pascal's Constants. *J. Chem. Educ.* **2008**, *85*, 532. [[CrossRef](#)]



© 2018 by the authors. Licensee MDPI, Basel, Switzerland. This article is an open access article distributed under the terms and conditions of the Creative Commons Attribution (CC BY) license (<http://creativecommons.org/licenses/by/4.0/>).